Research Square

Preprints are preliminary reports that have not undergone peer review.
They should not be considered conclusive, used to inform clinical practice,
or referenced by the media as validated information.

Development of immunostimulatory nanoparticles from ginseng powder to inhibit pulmonary metastasis

Daisuke Sasaki
Tokyo University of Science
Chiho Miyagi
Tokyo University of Science
Hironobu Kato
Tokyo University of Science
Kosuke Kusamori
Tokyo University of Science
Shoko Itakura
Tokyo University of Science
Yu Cai
Jinan University
Noriyasu Hada
Tokyo University of Science
Yoshihiro Nakajima
National Institute of Advanced Industrial Science and Technology (AIST)
Makiya Nishikawa
makiya@rs.tus.ac.jp

Tokyo University of Science

Research Article

Keywords: ginseng, plant-derived nanoparticles, immunostimulation, macrophage polarization, cancer immunotherapy

Posted Date: November 23rd, 2026

DOI: https://doi.org/10.21203/rs.3.rs-11674282/v1

License: This work is licensed under a Creative Commons Attribution 4.0 International License.
Read Full License

Additional Declarations: No competing interests reported.

Development of immunostimulatory nanoparticles from ginseng powder to inhibit pulmonary metastasis

Daisuke Sasaki[a,b], Chiho Miyagi[a], Hironobu Kato[a], Kosuke Kusamori[c,d], Shoko Itakura[a,d], Yu Cai[e], Noriyasu Hada[f], Yoshihiro Nakajima[b], and Makiya Nishikawa[a,d]*

[a] Laboratory of Biopharmaceutics, Faculty of Pharmaceutical Sciences, Tokyo University of Science, 6-3-1 Niijuku, Katsushika-ku, Tokyo 125-8585, Japan

[b] Cellular Function Analysis Research Group, Health and Medical Research Institute, National Institute of Advanced Industrial Science and Technology (AIST), 2217-14 Hayashi-cho, Takamatsu, Kagawa 761-0395, Japan

[c] Laboratory of Cellular Drug Discovery and Development, Faculty of Pharmaceutical Sciences, Tokyo University of Science, 6-3-1 Niijuku, Katsushika-ku, Tokyo 125-8585, Japan

[d] Research Institute for Science and Technology, Tokyo University of Science, 2641 Yamazaki, Noda, Chiba 278-8510, Japan

[e] School of Pharmacy, Jinan University, Guangzhou, Guangdong 510632, China

[f] Laboratory of Pharmacognosy, Faculty of Pharmaceutical Sciences, Tokyo University of

19 Science, 6-3-1 Niijuku, Katsushika-ku, Tokyo 125-8585, Japan

20

21 ***Corresponding author:**

22 Makiya Nishikawa, Ph.D.

23 Tel.: +81-3-5876-1564

24 Fax.: +81-3-5876-1564

25 E-mail address: makiya@rs.tus.ac.jp

26

ABSTRACT

Plant-derived nanoparticles, typically obtained from fresh plant materials, have attracted considerable attention for their therapeutic potential owing to their inherent biological activities. Although nanoparticles derived from fresh ginseng have been previously reported, no studies have examined nanoparticles formulated from ginseng powder, which is a more widely available and commercially distributed form. In this study, we developed nanoparticles from ginseng powder (gpNPs) and evaluated their physicochemical properties and biological functions. Ginseng powder was homogenized, centrifuged, filtered through a 0.45-μm syringe filter, and ultracentrifuged to obtain gpNPs. The resulting particles exhibited a uniform size distribution (50–200 nm) and negative surface charge. gpNPs were efficiently internalized by macrophage-like RAW264.7 cells and promoted cell proliferation. Furthermore, gpNPs upregulated the expression of inflammatory cytokines and M1 macrophage markers. Following intraperitoneal administration in mice, gpNPs enhanced the expression of inflammatory cytokines and costimulatory molecules CD80 and CD86 in the spleen. Importantly, gpNPs significantly suppressed the pulmonary metastasis of melanoma cells in a mouse model without causing notable toxicity. Collectively, these findings demonstrate that nanoparticles can be successfully

formulated from ginseng powder and exhibit potent immunostimulatory and anti-metastatic activities both *in vitro* and *in vivo*. Thus, gpNPs are promising nanoparticulate formulations for cancer immunotherapy.

Keywords: ginseng, plant-derived nanoparticles, immunostimulation, macrophage polarization, cancer immunotherapy

1. Introduction

Ginseng, the dried root of *Panax ginseng* C. A. Meyer (Araliaceae), has long been used in traditional medicine and contains numerous pharmacologically active constituents, including saponins, polyphenols, polysaccharides, and amino acids (1, 2). Recent studies have demonstrated its efficacy in treating various diseases such as cancer and inflammatory disorders (3, 4, 5). Between 1979 and 2018, 308 clinical trials of ginseng were registered, including 12 that focused on cancer treatment (6). Among its bioactive constituents, ginsenosides and polysaccharides have shown anti-cancer and immunomodulatory properties and function as immune enhancers or adjuvants (7). For example, ginsenoside Rg3 suppresses the proliferation, migration, invasion, and tube formation of cervical cancer cells by downregulating AKT2 (8). Ginsenoside Rh2 also inhibits breast cancer progression by enhancing natural killer (NK) cell-mediated immune responses (9). Ginseng polysaccharides exhibit significant anti-cancer and immunomodulatory effects in Lewis lung carcinoma-bearing mice by enhancing immune organ indices, T cell activity, cytokine production, and NK cell function (10).

Plant-derived nanoparticles (pdNPs) have emerged as promising drug delivery platforms owing to their biocompatibility, simple preparation, sustainability, low cost, and minimal toxicity (11, 12). Various pdNPs have been studied for disease treatment

(13, 14, 15). Since the first report of ginseng-derived pdNPs in 2019 (16), numerous studies have explored the potential of ginseng-derived nanoparticles in diverse therapeutic areas, including cancer treatment (17, 18, 19, 20, 21), skin protection and wound healing (22, 23, 24), and anti-inflammatory therapy (25, 26, 27, 28). Notably, some ginseng-derived nanoparticles modulate macrophage polarization and promote antitumor immune responses (18, 19). However, all previous studies utilized fresh ginseng, which is less stable during preservation and less accessible than the dried forms commonly used in clinical and commercial settings. To date, no studies have investigated pdNPs derived from dried ginseng.

In the present study, we successfully formulated immunostimulatory nanoparticles from commercially available ginseng powder (gpNPs) and characterized their physicochemical and biological properties, including immunostimulatory effects. To evaluate the therapeutic potential, we used a murine model of melanoma pulmonary metastasis, which is frequently employed in cancer immunotherapy research.

2. Methods

2.1. Materials

Fetal bovine serum (FBS) was obtained from Biosera (East Sussex, UK). Sodium phosphotungstate was obtained from Nacalai Tesque (Kyoto, Japan). Dulbecco's modified Eagle's medium (DMEM) and Roswell Park Memorial Institute (RPMI) 1640 medium were purchased from Shimadzu Diagnostics Corporation (Tokyo, Japan). Penicillin-streptomycin-L-glutamine solution (100×; PSG), methyl-β-cyclodextrin (MβCD), chlorpromazine (CPZ), ethylisopropyl amiloride 3-amino-N-(aminoiminomethyl)-6-chloro-5-[ethyl(1-methylethyl)amino]-2-pyrazinecarboxamide (EIPA), filipin III, fucoidan, and low-molecular or high-molecular dextran sodium sulfate (DSS-L or DSS-H) was obtained from FUJIFILM Wako Pure Chemical Corporation (Osaka, Japan). Lipopolysaccharide (LPS) from *Escherichia coli* O111:B4 was purchased from Sigma-Aldrich (St. Louis, MO, USA). All other chemicals used were of the highest commercially available grade.

2.2. Animals

Six-week-old male C57BL/6N mice were purchased from Sankyo Labo Service, Inc. (Tokyo, Japan) and maintained under specific pathogen-free conditions. All animal

experimental protocols were approved by the Institutional Animal Experimentation Committee of Tokyo University of Science (approval No. Y22015). All experiments were conducted in accordance with the principles outlined in the National Institutes of Health Guide for the Care and Use of Laboratory Animals and the ARRIVE guidelines.

2.3. Cell culture

The murine macrophage-like cell line RAW264.7 was obtained from Professor Yoshinobu Takakura (Hakubi Center, Kyoto University, Kyoto, Japan). RAW264.7 was cultured in RPMI medium supplemented with 10% heat-inactivated FBS and PSG at 37°C in a humidified atmosphere containing 5% CO_2. The murine fibroblast cell line NIH3T3 (RCB2767) was provided by Riken BRC through the National BioResource Project of MEXT/AMED (Ibaraki, Japan). The murine melanoma cell line, B16-BL6, was obtained from the Cancer Chemotherapy Center of the Japanese Foundation for Cancer Research (Tokyo, Japan). B16-BL6 cells expressing firefly luciferase (B16-BL6/FLuc) (29) were kindly provided by Professor Yoshinobu Takakura. NIH3T3, B16-BL6, and B16-BL6/FLuc cells were cultured in DMEM supplemented with 10% heat-inactivated FBS and subjected to PSG under the same conditions.

2.4. Preparation of gpNPs

The dried ginseng (lot. 008621009) was purchased from Tochimoto Tenkaido (Osaka, Japan) and crushed using a Wonder Crusher WC-3 (Osaka Chemical, Osaka, Japan). The powder (2.5 g) was suspended in 30 mL PBS and incubated for 6 h at room temperature (approximately 22°C). After incubation, the mixture was homogenized to obtain ginseng powder homogenate. The homogenate was centrifuged at 10,000×*g* for 1 h at 4°C. The resulting supernatant was passed through a 0.45-μm pore-size syringe filter (Minisart NML, Sartorius, Göttingen, Germany) to remove coarse residues. A 25 mL aliquot of the filtrate was then ultracentrifuged at 100,000×*g* for 120 min at 4°C using an Optima XL-K ultracentrifuge equipped with a 70 Ti rotor (Beckman Coulter, Brea, CA, USA). The resulting pellet was resuspended in 1 mL of PBS and further filtered through a 0.22-μm pore-size syringe filter (Minisart NML) to obtain gpNPs. The supernatant obtained after ultracentrifugation (gp-sup) was collected and used as a comparative control in subsequent experiments.

2.5. Characterization of gpNPs

The particle size and zeta potential of the gpNPs were measured by dynamic light scattering (DLS) using an ELSZ-2000ZS instrument (Otsuka Electronics, Osaka,

Japan). The particle size distribution was further analyzed by nanoparticle tracking analysis (NTA) using NanoSight NS300 (Malvern Panalytical, Malvern, United Kingdom). For transmission electron microscopy (TEM) imaging, a drop of gpNP suspension was placed onto a carbon-coated copper grid, negatively stained with 1% sodium phosphotungstate for 1 min, and air-dried at room temperature (approximately 20°C). The samples were then observed using a H-7650 TEM (Hitachi High-Tech, Tokyo, Japan) operated at 100 kV. To check their stability, gpNPs were suspended in PBS and stored at either room temperature (RT), 4°C, −30°C, or −80°C for 2 weeks. On days 0, 1, 2, 3, 7, and 14, the particle size and number of gpNPs were analyzed by NTA using NanoSight NS300, and the zeta potential was measured by DLS using an ELSZ-2000ZS instrument.

2.6. Effect of gpNPs on cell proliferation

NIH3T3, B16-BL6, and RAW264.7 cells were seeded into 96-well culture plates at a density of 5×10^3 cells/well and incubated for 24 h at 37°C. The culture medium was replaced with fresh medium containing various protein concentrations of gpNPs. After 24 h of incubation, the cell number was measured using a Cell Counting Kit-8 (CCK-8) (Dojindo Laboratories, Kumamoto, Japan). Cellular morphology at 0 and 100 μg/mL

gpNPs were observed using a BZ-9000 or BZ-X800 microscope. The protein concentrations in the gpNP samples were determined using a BCA assay kit (Thermo Fisher Scientific, Waltham, MA, USA).

2.7. Cellular uptake of DiO- or DiI-labeled gpNPs

The gpNPs were labeled with the red fluorescent lipophilic dye, 1,1′-dioctadecyl-3,3,3′,3′-tetramethylindocarbocyanine perchlorate (DiI; PromoCell GmbH, Heidelberg, Germany). Briefly, 0.1 mg/mL DiI solution (5 μL) was added to 500 μg/mL gpNPs (1 mL), and the mixture was incubated for 30 min at 37°C. Labeled gpNPs were purified by ultracentrifugation at 100,000×*g* for 120 min at 4°C to obtain purified DiI-labeled gpNPs (DiI-gpNPs). For confocal microscopy, NIH3T3, B16-BL6, and RAW264.7 cells were seeded onto an eight-well chambered cover glass (Iwaki; AGC Techno Glass, Chiba, Japan) at a density of 1×10^4 cells/well and cultured overnight at 37°C. The medium was then replaced with fresh culture medium containing 50 μg/mL DiI-gpNPs. After 12 h of incubation, the cells were fixed with 4% paraformaldehyde (PFA) on ice for 30 min and washed three times with PBS. Vectashield Antifade Mounting Medium with DAPI (Vector Laboratories, Burlingame, CA, USA) was used, and the samples were observed using a Leica SP8 laser scanning confocal microscope (Leica

Microsystems, Wetzlar, Germany) with LAS X Life Science software. For flow cytometric analysis, gpNPs were labeled with the green fluorescent lipophilic dye, 3,3′-dioctadecyloxacarbocyanine perchlorates (DiO; PromoCell GmbH), and purified as described above to yield DiO-labeled gpNPs (DiO-gpNPs). The cells were then incubated in fresh medium containing 0, 10, or 50 μg/mL DiO-gpNPs. After 3, 6, 12, and 24 h of incubation, the cells were fixed with 4% PFA, harvested using a cell scraper, and passed through a 70-μm cell strainer (Corning Incorporated, Corning, NY, USA). Quantitative analysis of the cellular uptake was performed using a BD FACSLyric flow cytometer (Becton, Dickinson and Company, Franklin Lakes, NJ, USA) and FlowJo software (ver8.7; Becton, Dickinson and Company).

2.8. Endocytosis inhibition assay

To elucidate the cellular uptake pathways of gpNPs in RAW264.7 cells, various endocytosis inhibitors were added, and the uptake of DiI-gpNPs was quantitatively evaluated. First, to determine the appropriate concentrations of endocytosis inhibitors, RAW264.7 cells were seeded into 96-well plates at a density of 5×10^3 cells/well and incubated at 37°C for 24 h. The medium was then replaced with fresh culture medium containing various concentrations of endocytosis inhibitors, MβCD, CPZ, EIPA, filipin

III, fucoidan, DSS-L, and DSS-H. After 24 h of incubation, cell number was assessed using a CCK-8 assay. The maximum concentration at which cell viability remained >80% was defined as the optimal concentration for each inhibitor. For fucoidan and DSS, a concentration of 0.5 mg/mL was used based on a previous report (30). Next, RAW264.7 cells were seeded in 12-well plates at a density of 1×10^5 cells/well and cultured at 37°C for 24 h. The medium was then replaced with fresh medium containing DiI-gpNPs in the presence of each endocytosis inhibitor. After 24 h, cells were harvested using a cell scraper and passed through a 70-μm cell strainer (Corning Incorporated). Quantitative analysis of the cellular uptake was performed using a BD FACSMelody flow cytometer (Becton, Dickinson and Company) and FlowJo software (ver8.7; Becton, Dickinson and Company).

2.9. RNA extraction and quantitative real-time RT-PCR

RAW264.7 cells were seeded in 6-well culture plates at a density of 1×10^5 cells/well and incubated for 24 h at 37°C. The culture medium was replaced with a fresh medium containing gpNPs at either 1×10^{10} particles/mL (low) or 5×10^{10} particles/mL (high). After 24 h of incubation, total RNA was extracted using Sepasol®RNA I Super G (Nacalai Tesque) according to the manufacturer's instructions. RNA concentration was

measured using a NanoDrop 2000 spectrophotometer (Thermo Fisher Scientific). Complementary DNA (cDNA) was synthesized from 10 ng total RNA using ReverTra Ace® qPCR RT Master Mix (Toyobo, Osaka, Japan). Reverse transcription was performed at 37°C for 15 min, followed by enzyme inactivation at 85°C for 5 s. Quantitative real-time RT-PCR (qRT-PCR) was performed using Thunderbird®SYBR™qPCR Mix (Toyobo) and the gene-specific primers listed in Supplementary Table S1. The PCR protocol consisted of an initial denaturation at 95°C for 30 s, followed by 65 amplification cycles, each comprising 95°C for 5 s, 55°C for 15 s, and 72°C for 45 s. GAPDH was used as the internal control. The threshold cycle (Ct) values for target genes were normalized to GAPDH (ΔCt), and relative expression levels were calculated using the comparative Ct ($2^{-\Delta\Delta Ct}$) method. For analysis of spleen samples, C57BL/6N mice were intraperitoneally injected with PBS (vehicle), LPS (50 ng/injection), gp-sup (500 μg protein/injection), or gpNPs (500 μg protein/injection). At 6 h post-injection, the mice were euthanized under isoflurane anesthesia and the spleen was collected. Spleen tissues were homogenized using a tissue homogenizer, and the homogenates were centrifuged at 10,000×*g* for 10 min. Total RNA was extracted using Sepasol®RNA I Super G as described above. cDNA synthesis and qRT-PCR were performed following the same protocol as described above.

228

229 **2.10. TNF-α release using ELISA**

230 RAW264.7 cells were seeded in 96-well culture plates at a density of 5×10^3 cells/well
231 and incubated for 24 h at 37°C. The culture medium was then replaced with fresh
232 medium containing various concentrations of gpNPs, gp-sup (100 μg protein/mL), and
233 Proteinase K (ProK)-treated gpNPs. gpNPs (100 μg/mL) were incubated with ProK (1
234 mg/mL) at 50 °C for 1 h, followed by ultrafiltration using an Amicon® Ultra Centrifugal
235 Filter (100 kDa MWCO; Merck KGaA, Darmstadt, Germany) to purify ProK-treated
236 gpNPs. After 24 h of incubation, the culture supernatants were collected, and TNF-α
237 levels were quantified using the Mouse TNF-α ELISA MAX™ Deluxe Set (BioLegend,
238 San Diego, CA, USA). For serum sample analysis, C57BL/6N mice were
239 intraperitoneally injected with one of the following: PBS (vehicle), LPS (50
240 ng/injection), gp-sup (500 μg protein/injection), ginseng decoction (100 mg/mL, 100 or
241 500 μL/injection), or gpNPs (500 μg protein/injection). At 6 h post-injection, the mice
242 were euthanized under isoflurane anesthesia, and blood was collected from the vena
243 cava. The blood samples were incubated at 4 °C overnight, followed by centrifugation
244 at 10,000×*g* for 10 min to obtain serum. Serum samples were stored at –80°C until
245 analysis. Serum TNF-α concentrations were measured using the ELISA kit and protocol

described above.

2.11. Reporter assay

RAW-Blue™ cells (InvivoGen, San Diego, CA, USA), which stably express a secreted embryonic alkaline phosphatase (SEAP) reporter gene under the control of nuclear factor-kappa B (NF-κB)/activator protein-1 (AP-1), were cultured according to the manufacturer's instructions. Cells were seeded in 96-well culture plates at a density of 1×10^4 cells/well in DMEM supplemented with Normocin™ (100 μg/mL) and incubated at 37°C in a humidified atmosphere with 5% CO_2. The medium was then replaced with fresh medium containing gpNPs or LPS, with or without the TLR4 antagonist TAK242 (ChemScene, Monmouth Junction, NJ, USA). After 24 h, 50 μL of culture supernatant was mixed with QUANTI-Blue™ (InvivoGen) and incubated at 37°C for 2 h. SEAP activity was determined by measuring absorbance at 600 nm.

NF-κB activation was also evaluated using HepG2 cells engineered to express dual luciferase reporters (NF-κB-HepG2 cells) as previously described (31). Cells were seeded in 96-well white clear-bottom plates (ThermoFisher Scientific) at a density of 3×10^4 cells/well and incubated for 24 h at 37°C. The medium was replaced with phenol red-free DMEM (ThermoFisher Scientific) supplemented with 10% FBS, 4 mM

glutamine, non-essential amino acids (ThermoFisher Scientific), 1 mM pyruvate (FUJIFILM Wako Pure Chemical Corporation), 25 mM HEPES/NaOH (pH 7.0, Nacalai Tesque), and 300 μM D-luciferin (Resem B.V., Lijnden, The Netherlands) with various concentrations of gpNPs. Bioluminescence was recorded every ~30 min for 5 s at 37°C under 5% CO_2 using a microplate luminometer (WSL-1565 Kronos HT, ATTO, Tokyo, Japan), with or without an R62 long-pass filter (HOYA, Tokyo, Japan). Luminescence from ELuc and SLR3 was quantified as described previously (32).

2.12. Tissue distribution of gpNPs following intraperitoneal injection in mice

The gpNPs were labeled with the near-infrared fluorescent lipophilic dye, 1,1′-dioctadecyl-3,3,3′,3′-tetramethylindotricarbocyanine iodide (DiR; ThermoFisher Scientific). DiR-labeled gpNPs (DiR-gpNPs) were prepared as described above. C57BL/6N mice were intraperitoneally injected with either DiR-gpNPs (500 μg/mouse) or free DiR dye (0.5 μg/mouse). At 1, 3, 6, 12, and 24 h post-injection, the mice were anesthetized with isoflurane and imaged *in vivo* using an IVIS imaging system (Revvity, Waltham, MA, USA). After 24 h post-injection, the mice were euthanized under isoflurane anesthesia, and the major organs were harvested for *ex vivo* imaging. Fluorescence signals in the organs were visualized using an IVIS imaging system.

282

283 **2.13. Anti-cancer effect of gpNPs in lung metastasis mouse model**

284 To establish a mouse model of lung metastasis, B16-BL6/FLuc cells suspended in PBS

285 (2×10^5 cells/100 μL) were injected intravenously into C57BL/6N mice. The following

286 day, the mice were randomly divided into two treatment groups and administered either

287 PBS (vehicle control) or gpNPs (500 μg protein/injection) via intraperitoneal injection

288 once every three days. On day 17 after cell transplantation, the mice were anesthetized

289 with isoflurane, and 200 μL (3 mg) of VivoGlo™ Luciferin In Vivo Grade (Promega,

290 Madison, WI, USA) was directly injected into the lungs. Luciferase activity was

291 detected using an IVIS imaging system. Following imaging, the mice were euthanized

292 with isoflurane, and the lungs were collected and fixed in 4% PFA for quantification of

293 metastatic colonies. To evaluate the potential adverse effects of gpNP treatment, serum

294 aspartate aminotransferase (AST) and alanine aminotransferase (ALT) levels were

295 assessed as indicators of hepatotoxicity, and creatinine (Cre) levels were assessed as

296 indicators of nephrotoxicity. After 17 days of treatment, the mice were sacrificed, and

297 peripheral blood was collected. Blood samples were stored at 4°C overnight and

298 centrifuged at 10,000×*g* for 10 min to obtain serum, which was stored at -80°C until

299 analysis. Serum AST and ALT levels were measured using a transaminase CII test Wako

kit (FUJIFILM Wako Pure Chemical), and serum Cre levels were measured using a LabAssay Creatinine kit (FUJIFILM Wako Pure Chemical).

2.14. Statistical analysis

Statistical differences were evaluated using one-way analysis of variance (ANOVA), followed by Dunnett's post-hoc test for multiple comparisons or Student's *t*-test for comparisons between two groups. Differences were considered statistically significant at $p < 0.05$. Statistical analysis was performed using software EZR (Easy R) v1.64 (33).

3. Results

3.1. Physicochemical characterization of gpNPs

Fig. 1A illustrates the preparation of gpNPs from ginseng powder by ultracentrifugation. TEM revealed that the gpNPs were spherical (Fig. 1B, yellow arrows). NTA showed a main peak at 82 nm with a size distribution ranging from approximately 50 to 300 nm in diameter (Fig. 1C). DLS analysis revealed that the gpNPs had an average particle size of 89.4 ± 11.3 nm and a zeta potential of −12.3 ± 1.8 mV. Furthermore, although the zeta potential slightly decreased during the two-week storage period at RT, no significant changes were observed in either the particle size or the particle number (Fig. S1).

3.2. Proliferation and cellular uptake in cultured cell lines

The effects of the gpNPs on cell proliferation were evaluated. Fig. 2A shows the number of NIH3T3, B16-BL6, and RAW264.7 cells after 24 h of incubation with gpNPs at varying protein concentrations. The addition of gpNPs had minimal effect on the number of NIH3T3 and B16-BL6 cells, even at high concentrations. In contrast, gpNPs increased the number of RAW264.7 cells. As shown in Fig. 2B, a significant increase in RAW264.7 cell number was observed at a gpNP concentration of 100 μg/mL, consistent with the findings in Fig. 2A.

Confocal microscopy images (Fig. 2C) showed that the red fluorescence signals derived from DiI-gpNPs were observed in RAW264.7 cells in both a time- and concentration-dependent manner, whereas no notable uptake was observed in NIH3T3 or B16-BL6 cells. These results indicated that gpNPs were preferentially and efficiently taken up by RAW264.7 cells. The uptake of DiI-gpNPs by RAW264.7 cells was reduced by approximately 22%, 12%, and 62%, in the presence of the class A scavenger receptor inhibitors fucoidan, DSS-L, and DSS-H, respectively (Fig.2E).

3.3. Immunostimulatory effect of gpNPs on RAW264.7 cells

Because gpNPs promoted cell proliferation and were efficiently taken up by RAW264.7 cells, subsequent experiments were conducted using gpNP-treated RAW264.7 cells. As shown in Fig. 3A, gene expression levels were examined following treatment with gpNPs or LPS. LPS treatment significantly increased the mRNA expression of M1 markers (*iNOS*, *TNF-α*, *IL-6*, and *IL-1β*), with minimal changes in M2 markers (*Arg-1* and *IL-10*). Similarly, gpNP treatment induced concentration-dependent upregulation of M1 marker expression. In contrast, among the M2 markers, IL-10 expression moderately increased only at the highest gpNP concentration, whereas the overall M2 marker expression remained largely unchanged.

To further evaluate the immunostimulatory properties of gpNPs, TNF-α production was assessed in cells treated with gpNPs, gp-sup (supernatant obtained after ultracentrifugation), and proteinase K-treated gpNPs, which inactivate ginseng-derived nanoparticles (16). Consistent with the gene expression data shown in Fig. 3A, gpNPs induced a concentration-dependent increase in TNF-α production, whereas TNF-α levels were lower in both the gp-sup-and proteinase K-treated gpNP groups (Fig. 3B).

To elucidate the mechanism underlying the immunostimulatory activity of gpNPs, reporter assays were performed using RAW-Blue™ cells, which secrete SEAP in response to NF-κB activation. Treatment with gpNPs increased SEAP activity in a concentration-dependent manner. Furthermore, co-treatment with TAK242, a TLR4 inhibitor, reduced SEAP activity (Fig. 3C). In contrast, NF-κB-HepG2 cells, which express low levels of TLR4, showed no response to gpNP treatment, suggesting that gpNPs activate the TLR4/NF-κB signaling pathway (Fig. S3A, B).

3.4. *In vivo* immunostimulatory effect following intraperitoneal administration of gpNPs

Next, the immunostimulatory effects of gpNPs were evaluated *in vivo*. In addition to TNF-α, the dendritic cell activation markers CD80 and CD86 were also evaluated. As

363 shown in Fig. 4A, intraperitoneal administration of LPS upregulated the mRNA
364 expression of TNF-α and CD86. Similarly, intraperitoneal administration of gpNPs
365 resulted in an even greater upregulation of these genes than LPS. In contrast, the
366 administration of gp-sup did not alter gene expression, which is consistent with the *in*
367 *vitro* findings. In accordance with the findings presented in Fig. 3A, while serum TNF-α
368 levels remained below the detection limit subsequent to the administration of gp-sup to
369 the mice, an increase in TNF-α levels was observed following the administration of
370 gpNPs (Fig. 4B). Furthermore, gpNP administration induced significantly higher TNF-α
371 production than ginseng decoction (Fig. 4C), which has immunostimulatory effects
372 (34). To assess tissue distribution, DiR-gpNPs or free DiR dye were administered
373 intraperitoneally, and fluorescence was monitored at various time points using IVIS
374 imaging (Fig. 4D). Three hours after injection, DiR-derived fluorescence was observed
375 throughout the abdomen in both groups, indicating the migration of DiR and DiR-
376 gpNPs from the abdominal cavity into blood circulation. Subsequently, stronger
377 fluorescence signal was detected in the DiR-gpNPs group than in the DiR group at
378 specific sites in the abdominal cavity, suggesting that DiR-gpNPs accumulated in major
379 organs, such as the liver, for up to 24 h. At 24 h post-injection, the major organs were
380 harvested for *ex vivo* imaging. In the free DiR dye-treated group, fluorescence was

primarily detected in the intestine, liver, and spleen. In contrast, the DiR-gpNP group exhibited prominent fluorescence signals in the liver and spleen, with a markedly higher intensity than that of the free DiR group.

3.5. Anti-cancer effect of gpNPs in a pulmonary metastasis mouse model

Given the immunostimulatory effects of gpNPs shown in Figs. 3 and 4, we evaluated their therapeutic potential in cancer. PBS or gpNPs were intraperitoneally administered to mice with pulmonary metastasis induced by the intravenous injection of B16-BL6/FLuc cells. On day 17 after transplantation, bioluminescence imaging was performed to assess tumor burden. As shown in Fig. 5A, the gpNP-treated group exhibited lower luminescence intensity derived from luciferase-expressing B16-BL6 cells than the PBS-treated group. In addition, the number of metastatic colonies in the lungs was markedly reduced in gpNP-treated groups (Fig. 5B and Supplementary Fig. S4). Throughout the treatment period, no significant differences in body weights were observed between the gpNP and PBS groups (Fig. 5C), suggesting that gpNP administration did not induce systemic toxicity. To further evaluate the potential adverse effects, serum levels of ALT and AST were measured as indicators of hepatotoxicity, and serum Cre was quantified as an indicator of nephrotoxicity. As shown in Fig. 5D-5F,

399 there were no significant differences in the ALT or Cre levels between the two groups.

400 Interestingly, the AST levels were significantly lower in the gpNP-treated group than in

401 the PBS-treated group.

402

403

4. Discussion

pdNPs have primarily been isolated from fresh plant materials (35, 36), and there have been no reports on the isolation of nanoparticles from dried ginseng. In this study, we successfully isolated gpNPs for the first time. Although two previous studies have reported the isolation of nanoparticles from dried plants (37, 38), both used hot water extraction, a process that may lead to the degradation of heat-sensitive components, such as proteins.

pdNPs carry a variety of surface proteins that play crucial roles in their cellular uptake and biological activities (35, 39, 40). Proteinase K treatment of nanoparticles derived from fresh ginseng significantly reduces their biological activity (16), which was also confirmed in the present study (Fig. 3B). These observations suggest that mild isolation conditions are essential for preserving the functional protein components and maintaining the biological activity of pdNPs.

Nanoparticles isolated from dried ginseng are thought to be challenging because of dehydration-induced disruption, but our findings suggest that polysaccharides, particularly pectin, help maintain the stability and preserve nanoparticles. Indeed, gpNPs exhibited excellent stability under both refrigerated and frozen storage conditions (Fig. S1). Pectin, a key component of plant cell walls, is

crucial for maintaining cell wall integrity (41). In *Myrothamnus flabellifolia*, the pectin-rich RG-I region containing arabinan helps to maintain cell wall flexibility under dehydration stress (42). Ginseng roots contain approximately 28.56% polysaccharides, including starch-like glucans and pectins (43). Ginseng's water-soluble pectin is primarily composed of homogalacturonan and RG-I domains, such as β-1,4-galactan and α-1,5-arabinan residues (44). We speculate that the pectin in ginseng helps maintain the nanoparticle structure during drying, enabling stable recovery from ginseng powder.

gpNPs significantly enhanced TNF-α production and cell proliferation in RAW264.7 macrophages (Figs. 2 and 3), likely through activation of TLR4 and the MyD88-dependent signaling cascade, leading to NF-κB activation (16). TLR4 signaling recruits MyD88 via TIRAP, activates IRAK-4 and IRAK-1, and triggers the phosphorylation of IKKβ and MAPK kinases, promoting the transcription of proinflammatory genes, such as TNF-α and IL-6 (45, 46). To assess NF-κB activation by gpNPs, NF-κB reporter cells were employed. Treatment of RAW-Blue™ cells with gpNPs resulted in a concentration-dependent increase in SEAP activity without detectable cytotoxicity (Fig. 3C and S2C). Furthermore, SEAP activity was reduced in the presence of the TLR4 inhibitor TAK242, which did not affect SEAP activity or cell viability in RAW-Blue™ cells (Fig. S2B). A similar response was observed with LPS, a

known TLR4 agonist (Fig. S2A). These findings suggest that gpNPs induce NF-κB activation in a TLR4-depenndent manner. In addition, NF-κB activation was evaluated using NF-κB-HepG2 cells, which express low levels of TLR4 (47). No significant NF-κB activation was observed in these cells (Fig. S3A, B), further supporting the involvement of TLR4 in gpNP-mediated signaling. Collectively, these results suggest that gpNPs promote cytokine production through the TLR4/MyD88/NF-κB signaling pathway.

NF-κB not only regulates cytokine expression (48, 49, 50), but also promotes cell proliferation via cyclin D1 induction (51) and enhances macrophage phagocytic activity (52). This suggests that gpNPs activate TLR4/NF-κB signaling to enhance cellular uptake and proliferation, as illustrated by the selective uptake of gpNPs by RAW264.7 cells (Fig. 2C, 2D). To further elucidate the mechanism of gpNP uptake by RAW264.7 cells, endocytosis inhibitors were used. As shown in Fig. 2E, CPZ increased the internalization of gpNPs, whereas fucoidan and DSS decreased it. Previous studies have reported that CPZ increased intracellular Ca^{2+} levels, which may enhance phagocytosis, as Ca^{2+} signaling promotes phagocytic cup formation and increases the efficiency of particle internalization (53, 54). Therefore, the CPZ-induced increase in gpNP uptake by RAW264.7 cells may be attributable to enhanced phagocytic activity.

458 On the other hand, the uptake was reduced by fucoidan and DSS, inhibitors of SR-A, a
459 receptor predominantly expressed on macrophages and dendritic cells (55). SR-A is
460 known to recognize a variety of negatively charged ligands, including oxidized low-
461 density lipoprotein, advanced glycation end products, apoptotic cells, LPS, DSS, and
462 fucoidan (56). This broad ligand recognition is attributable to its lysine-rich domain,
463 which facilitates binding through electrostatic interactions (57). Given that gpNPs are
464 negatively charged and are likely composed of ginseng-derived polysaccharides, these
465 findings suggest that gpNPs are preferentially internalized into RAW264.7 cells via an
466 SR-A-mediated pathway.

467 The addition of gpNPs to RAW264.7 cells significantly increased the
468 expression of M1 markers, while having minimal effect on M2 markers (Fig. 3A). M1
469 macrophages play a central role in antitumor immunity by secreting proinflammatory
470 cytokines such as TNF-α and IL-6 (58), whereas M2 macrophages contribute to tumor
471 progression and immune suppression (59, 60). The gpNPs promoted M1 marker
472 expression, while only modestly increasing the expression of the M2 marker IL-10 at
473 higher concentrations. IL-10 is upregulated in the inflammatory response as a regulatory
474 mechanism to avoid excessive immune activation (61, 62) Therefore, gpNPs may
475 provide balanced immune activation, inducing strong M1-type responses and negative

476 feedback mechanisms to control inflammation.

477 The gpNPs significantly suppressed tumor growth without any apparent
478 adverse effects (Fig. 5), likely owing to their potent immunostimulatory activity. The
479 murine model of melanoma pulmonary metastasis is widely used in cancer
480 immunotherapy research because of its immunogenicity (63, 64, 65) and abundance of
481 macrophages in the lungs (66, 67, 68). Therefore, this model is suitable for evaluating
482 gpNPs as a novel immunotherapeutic strategy. Cao *et al* reported that the administration
483 of 5,6-dimethylxanthenone-4-acetic acid (a TNF-α inducer) or LPS to tumor-bearing
484 mice enhanced TNF-α production in the spleen, liver, serum, and tumors, resulting in
485 tumor suppression (69, 70). Our data revealed that gpNPs accumulated primarily in the
486 liver and spleen, organs rich in macrophages (71, 72), and induced TNF-α expression
487 locally. Interestingly, only the gpNP-treated group exhibited detectable levels of TNF-α
488 in the serum, suggesting enhanced systemic immune activation compared to the ginseng
489 supernatant (gp-sup) group. As shown in Fig. 4D, intraperitoneally administered gpNPs
490 were transferred into blood circulation within approximately 3 h and then accumulated
491 in the liver and spleen. This suggests that gpNPs were not only taken up by
492 intraperitoneal macrophages but also distributed to immune cell-rich tissues (Fig. 4),
493 and activated immune cells to enhance TNF-α mRNA expression, leading to elevated

494 TNF-α and subsequent tumor suppression.

495 gpNPs also increased the expression of costimulatory molecules CD80 and
496 CD86 (Fig. 4), which are crucial for the activation of $CD4^+$ T cells (73). These markers
497 promote T cell-mediated cytotoxic responses, which are central to modern cancer
498 immunotherapies (74). Their expression is regulated by TLR/NF-κB signaling (75, 76),
499 linking gpNP treatment to both innate and adaptive immune activation. Ginseng
500 saponins and their metabolites enhance CD80/CD86 expression (77, 78), supporting our
501 findings. Although further investigation is needed to identify the specific components of
502 gpNPs responsible for these effects, current evidence supports the notion that gpNPs
503 upregulate CD80/86 expression, likely via TLR-dependent NF-κB activation. Taken
504 together, these findings suggest that gpNPs exert potent anti-cancer effects through two
505 mechanisms: (1) TNF-α-mediated cytokine activity and (2) activation of adaptive
506 immunity via CD80/86-driven T cell responses.

507

508 **5. Conclusions**

509 This study is the first to demonstrate that nanoparticles can be obtained from ginseng
510 powder, and that these gpNPs enhance the production of inflammatory cytokines both *in*
511 *vitro* and *in vivo*. Moreover, gpNPs significantly suppressed tumor growth in a mouse

model of pulmonary metastasis, likely through their immunostimulatory effects. These findings suggest that gpNPs are promising novel immunostimulants for cancer therapy.

Glossary

ALT, alanine aminotransferase; AP-1, activator protein-1; AST, aspartate aminotransferase; CCK-8, Cell Counting Kit-8; CPZ, chlorpromazine; Cre, creatinine; DiI, 1,1′-dioctadecyl-3,3,3′,3′-tetramethylindocarbocyanine perchlorate; DiO, 3,3′-dioctadecyloxacarbocyanine perchlorate; DiR, 1,1′-dioctadecyl-3,3,3′,3′-tetramethylindotricarbocyanine iodide; DLS, dynamic light scattering; DMEM, Dulbecco's modified Eagle's medium; DSS, dextran sodium sulfate; EIPA, ethylisopropyl amiloride 3-amino-N-(aminoiminomethyl)-6-chloro-5-[ethyl(1-methylethyl)amino]-2-pyrazinecarboxamide; FBS, fetal bovine serum; gpNP, ginseng powder-derived nanoparticle; LPS, lipopolysaccharide; MβCD, methyl-β-cyclodextrin; NF-κB, nuclear factor-kappa B; NTA, nanoparticle tracking analysis; pdNP, plant-derived nanoparticle; PFA, paraformaldehyde; ProK, proteinase K; PSG, penicillin-streptomycin-L-glutamine solution; qRT-PCR, quantitative real-time RT-PCR; RPMI, Roswell Park Memorial Institute; SEAP, secreted embryonic alkaline phosphatase; TEM, transmission electron microscopy; TK, thymidine kinase.

Ethics approval and consent to participate

All animal experimental protocols were approved by the Institutional Animal Experimentation Committee of Tokyo University of Science (approval No. Y22015). All experiments were conducted in accordance with the principles outlined in the National Institutes of Health Guide for the Care and Use of Laboratory Animals and the ARRIVE guidelines.

Availability of data and materials: All data are available on request.

Declaration of competing interest: The authors declare no conflicts of interest.

Funding: This research did not receive any specific grant from funding agencies in the public, commercial, or not-for-profit sectors.

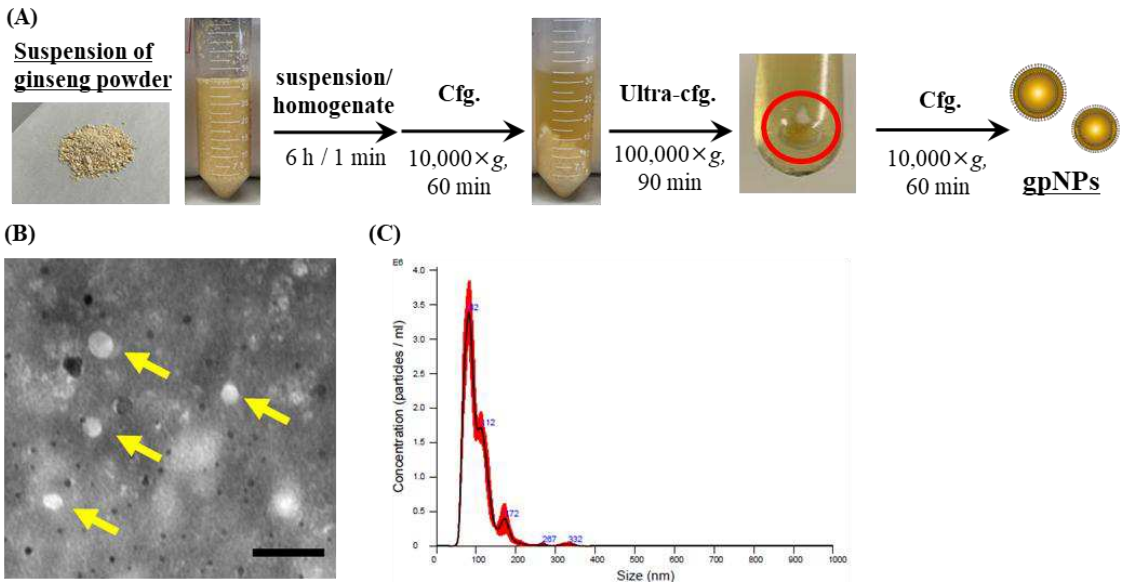
CRediT authorship contribution statement: Daisuke Sasaki: Conceptualization, Methodology, Investigation, Writing-Original Draft. **Chiho Miyagi**: Investigation, Writing-Review & Editing. **Hironobu Kato**: Investigation. **Kosuke Kusamori**: Conceptualization, Methodology, Validation, Writing-Review & Editing. **Shoko**

Itakura: Methodology, Validation, Writing-Review & Editing. **Yu Cai**: Writing-Review & Editing. **Noriyasu Hada**: Writing-Review & Editing. **Yoshihiro Nakajima**: Writing-Review & Editing. **Makiya Nishikawa**: Conceptualization, Methodology, Validation, Formal analysis, Writing-Review & Editing. All authors read and approved the final manuscript.

Acknowledgments: The authors are grateful to Koji Tsuchiya (Research Institute for Science and Technology, Tokyo University of Science) for their kind support with TEM imaging.

558

559 **Fig. 1**



560

561 **Fig. 1. Preparation and characterization of gpNPs.** (A) Schematic illustration of the

562 preparation process. Ginseng powder was soaked in PBS for 6 h, homogenized,

563 centrifuged (Cfg), filtered, and then ultracentrifugation (ultra-cfg) to obtain ginseng

564 powder-derived nanoparticles (gpNPs). (B) Transmission electron microscopy (TEM)

565 image of gpNPs. gpNPs were negatively stained with 1% sodium phosphotungstate and

566 imaged using an H-7650 transmission electron microscope. Scale bar = 200 nm. Yellow

567 arrows indicate gpNPs. (C) Size distribution of gpNPs. gpNPs were diluted in PBS, and

568 their size distribution was analyzed using a NanoSight NS300.

569

570

Fig. 2

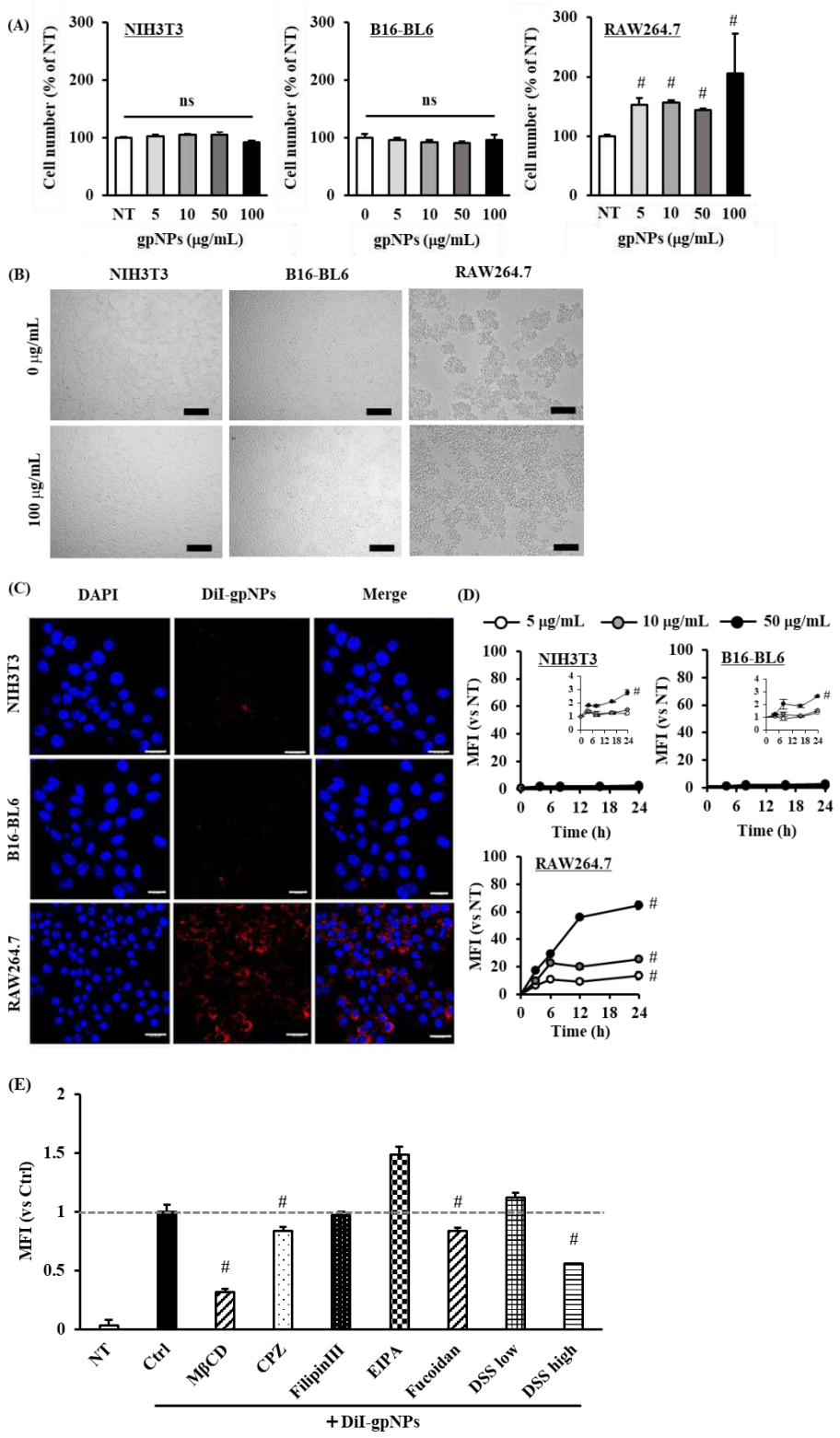


Fig. 2. Effects of gpNPs on cultured cell lines. (A) Cell number after gpNP treatment.

NIH3T3, B16-BL6, and RAW264.7 cells (5×10^3 cells/well) were seeded in 96-well culture plates and incubated for 24 h. Cells were then incubated with various concentrations of gpNPs for an additional 24 h, and cell number was measured using the CCK-8 assay. Results are expressed as mean ± SD (n=3). $^{\#}p<0.05$ vs. NT group. (B) Cell morphology after gpNP treatment. Cells (1×10^5 cells/well) were seeded in 12-well culture plates and incubated with 0 or 100 μg/mL of gpNPs for 24 h. Images were taken using a light microscope. Scale bars = 100 μm. (C) Cellular uptake visualized by confocal microscopy. Cells (1×10^4 cells/well) were seeded in 8-well chambered coverglass and incubated with 50 μg/mL of DiI-labeled gpNPs for 24 h, followed by fixation and DAPI staining. Confocal microscopy was used for imaging. Scale bars = 50 μm. (D) Time-dependent uptake of DiO-labeled gpNPs. NIH3T3, B16-BL6, and RAW264.7 cells (1×10^5 cells/well) were seeded in 12-well culture plates and incubated with DiO-gpNPs for 3, 6, 12, and 24 h, followed by fixation with paraformaldehyde. The fluorescence intensity of cells was quantified by flow cytometry, and the mean fluorescence intensity (MFI) was calculated. (E) Cellular uptake of DiI-labeled gpNPs under various endocytosis inhibitors. RAW264.7 cells were seeded in 12-well culture plates (1×10^5 cells/well) and incubated with DiI-gpNPs and endocytosis inhibitors for 24 h, followed by fixation with paraformaldehyde. The fluorescence intensity of cells

593 was quantified by flow cytometry, and the mean fluorescence intensity (MFI) against
594 the Ctrl was calculated. Results are expressed as mean ± SD (n=3). $^{\#}p<0.05$ vs. NT
595 group or Ctrl group. B16-BL6, murine melanoma cell line; Ctrl, Control; gpNPs,
596 ginseng powder-derived nanoparticles; NIH3T3, murine fibroblast cell line; ns, not
597 significant; NT, no treatment; RAW264.7, murine macrophage cell line.
598

Fig. 3

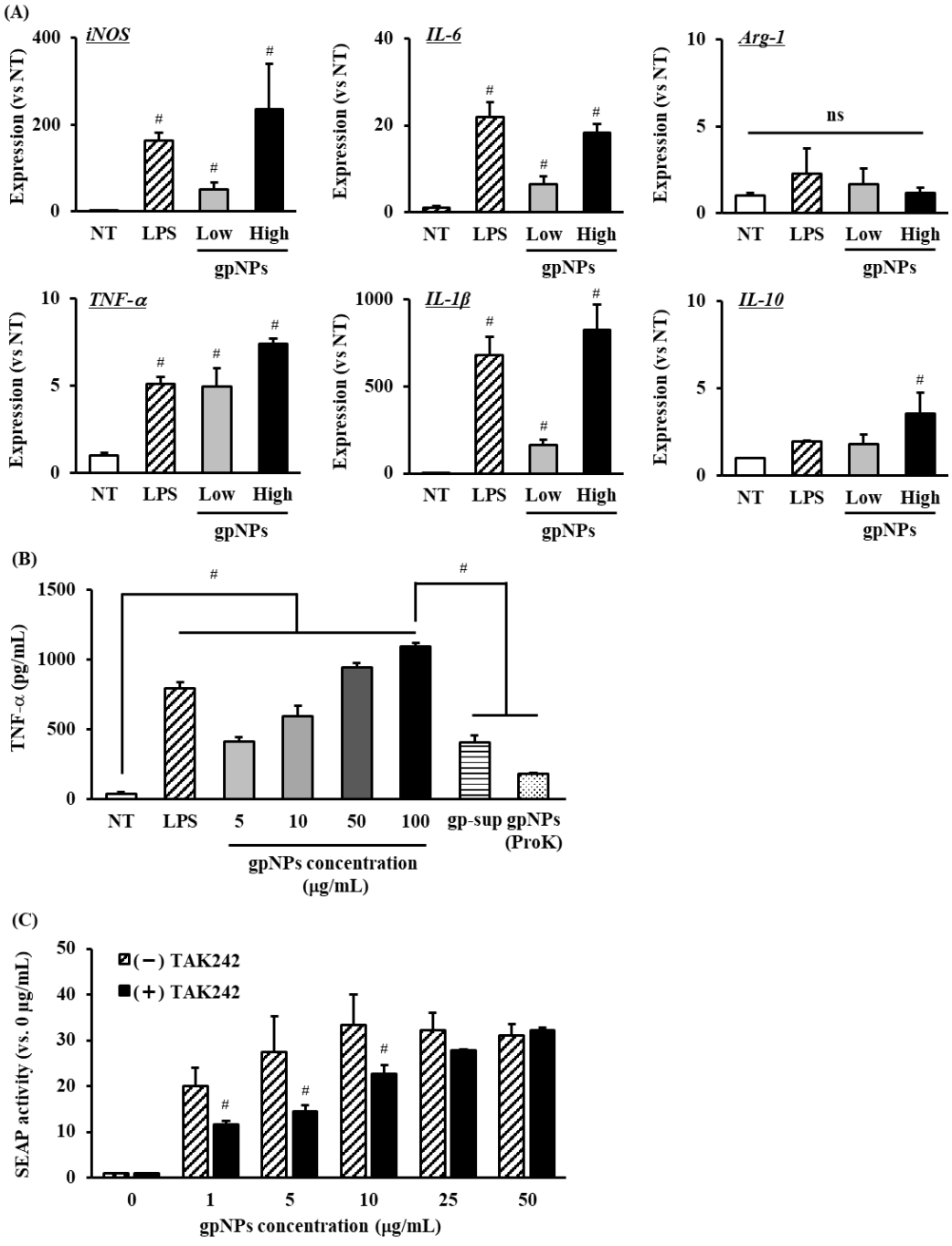
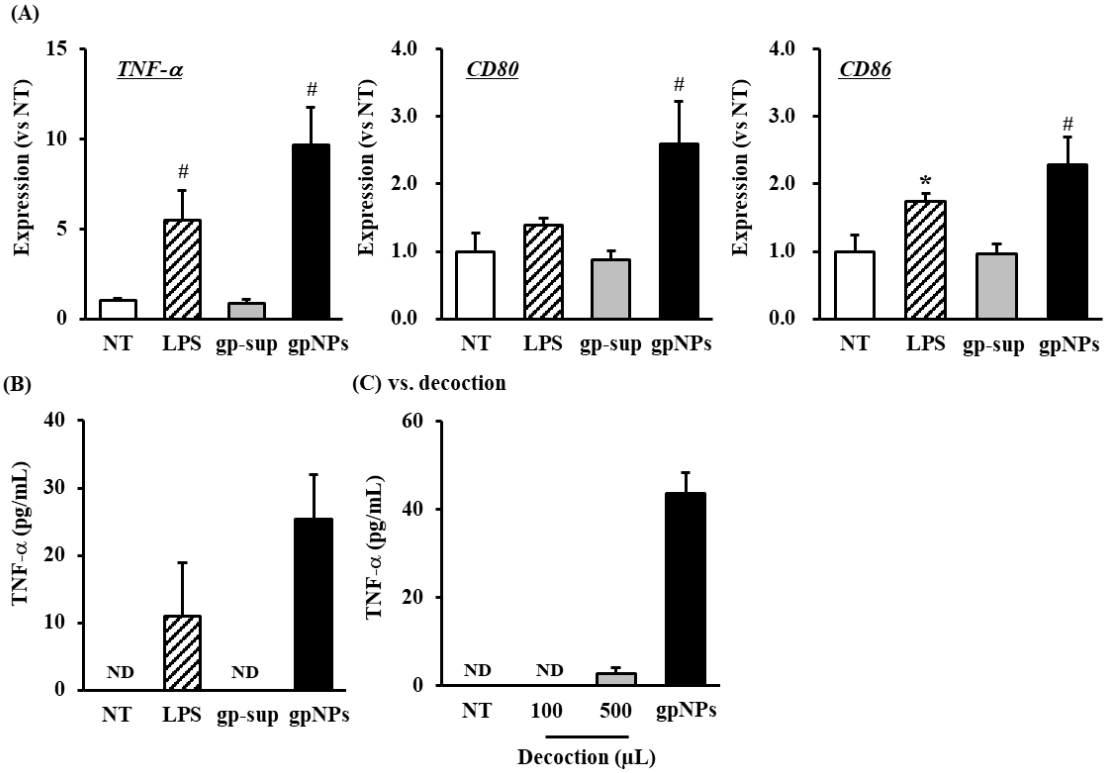
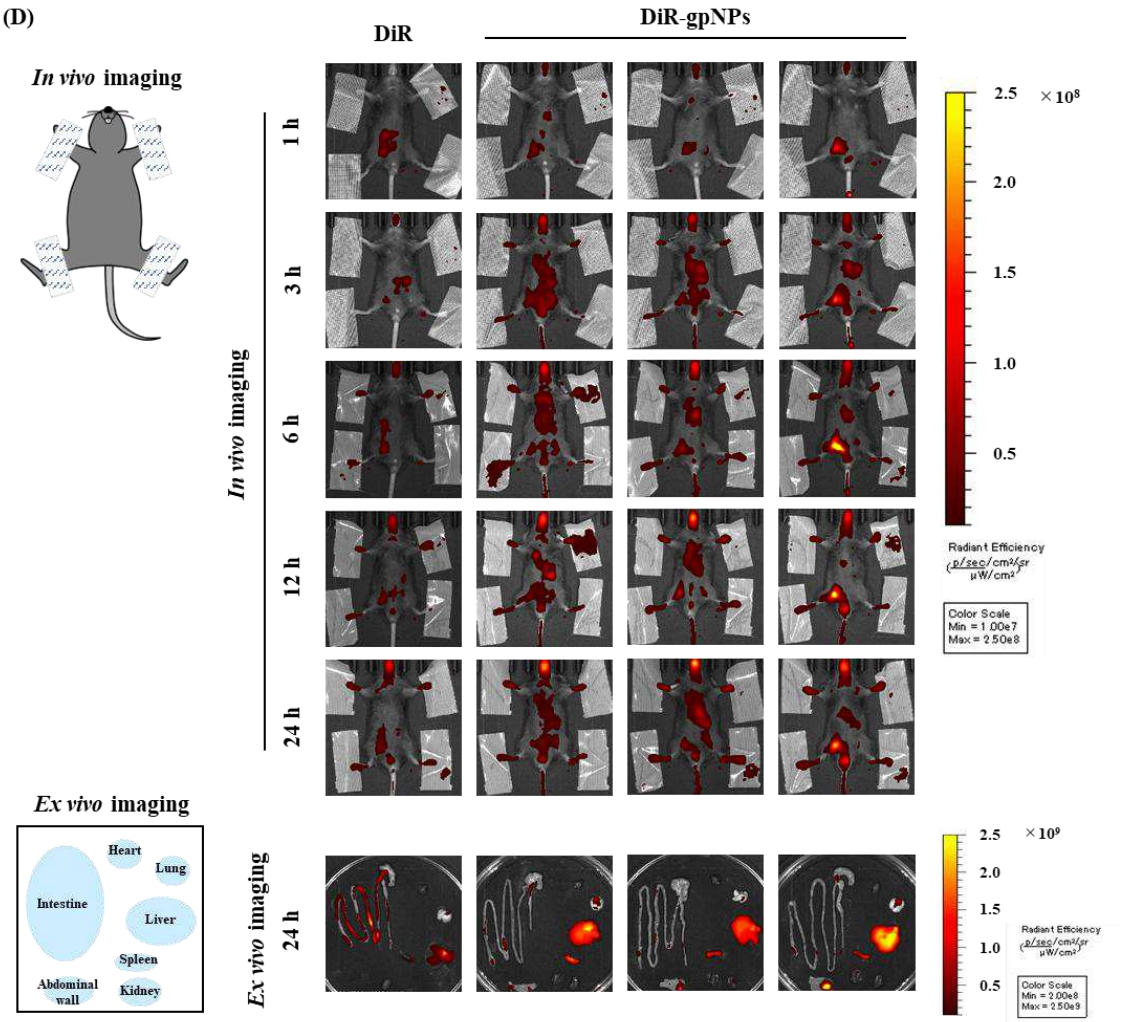


Fig. 3. Immunostimulatory activity of gpNPs in macrophages. (A) mRNA expression in RAW264.7 cells. RAW264.7 cells (1×10^5 cells/well) were seeded in 12-well culture plates and incubated with 50 μg/mL of gpNPs for 24 h. The mRNA

604 expression of *iNOS*, *IL-6*. *Arg-1, TNF-α*, *IL-1β*, and *IL-10* was analyzed using real-time
605 RT-PCR and normalized to GAPDH mRNA. Results are expressed as mean ± SD (n=3).
606 $^{\#}p<0.05$ vs. NT group. (B) TNF-α secretion. RAW264.7 cells (5×10^3 cells/well) were
607 seeded in 96-well culture plates and incubated for 24 h with 10 ng/mL of LPS, 5-100
608 μg/mL of gpNPs, 100 μg/mL of gp-sup, or 100 μg/mL of proteinase K (ProK)-treated
609 gpNPs. TNF-α levels in the supernatant were measured using an ELISA kit. (C) SEAP
610 activity. RAW-Blue™ cells were seeded in 96-well culture plates (1×10^4 cells/well) and
611 incubated with TAK242 for 2 h, followed by the addition of 1-50 μg/mL of gpNPs for
612 24 h. SEAP activity in the supernatant was measured using a QUANTI-Blue™. Results
613 are expressed as mean ± SD (n=3). $^{\#}p<0.05$. Arg-1, Arginase-1; gpNPs, ginseng powder-
614 derived nanoparticles; IL, Interleukin; LPS, lipopolysaccharide; NT, No treatment; ns,
615 not significant; RAW264.7, murine macrophage cell line; RT-PCR, reverse
616 transcription-polymerase chain reaction; SEAP, secreted embryonic alkaline
617 phosphatase; TNF-α, tumor necrosis factor-α.
618

Fig. 4


(A)
TNF-α
CD80
CD86
Expression (vs NT)
NT
LPS
gp-sup
gpNPs
(B)
TNF-α (pg/mL)
ND
(C) vs. decoction
100
500
Decoction (μL)



621

622 **Fig. 4. Effects of gpNPs following intraperitoneal administration in mice.** (A)

623 Splenic mRNA expression. Mice were intraperitoneally administered with gpNPs or gp-

624 sup (500 μg protein/dose), or LPS (50 ng/dose). Spleens were harvested 24 h post-

625 injection. mRNA levels of *TNF-α*, *CD80*, and *CD86* were evaluated by real-time RT-

626 PCR and normalized to GAPDH mRNA. Results are expressed as mean ± SEM (n=3).

627 $^{\#}p<0.05$ vs. NT group. (B) Serum TNF-α levels. TNF-α levels in serum collected 24 h

628 post-injection were measured using an ELISA kit. Results are expressed as mean ± SEM

(n=3). (C) Comparison with ginseng decoction. Mice were intraperitoneally administered with 500 μL of gpNPs (500 μg protein/shot) or 100 or 500 μL ginseng decoction. TNF-α levels in serum were measured 24 h later. Results are expressed as mean ± SEM (n=3). (D) Biodistribution of DiR-gpNPs. Mice were intraperitoneally administered with DiR-gpNPs or free DiR. Whole-body fluorescence was visualized at 1, 3, 6, 12, and 24 h post-injection using an *in vivo* imaging system. After 24 h, major organs were harvested and imaged *ex vivo*. gpNPs, ginseng powder-derived nanoparticles; LPS, lipopolysaccharide; ND, not detected; NT, No treatment; TNF-α, tumor necrosis factor-α

Fig. 5

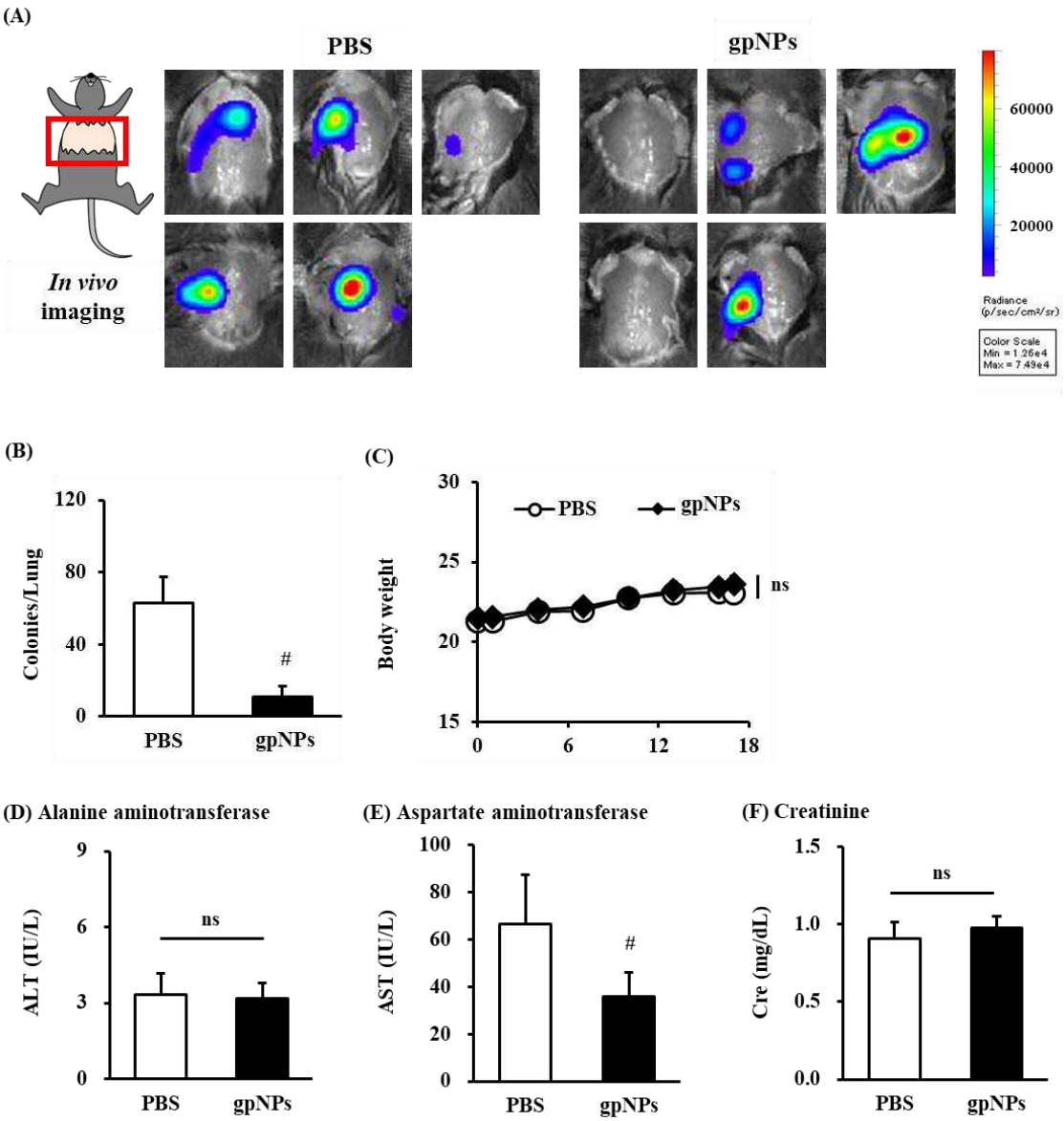


Fig. 5. Anticancer effects of gpNPs in a lung metastasis mouse model. (A) *In vivo* imaging. C57BL/6 mice were intravenously injected with B16-BL6/FLuc cells to establish a lung metastasis model. Mice received intraperitoneal injections of PBS (vehicle) or gpNPs (500 μg protein/dose) every three days. On day 17, mice were injected with VivoGlo™ Luciferin, and the luminescence was detected. (B)

Quantification of lung metastasis. On day 17, lungs were harvested, and visible melanoma colonies were counted. Results are expressed as mean ± SEM (n=5). #$p<0.05$ vs. PBS group. (C) Body weight monitoring. Mice were weighed every 3 days. Results are expressed as mean ± SEM (n=5). ns, not significant. (D-F) Serum biochemical analyses. Serum levels of (D) ALT (alanine aminotransferase), (E) AST (aspartate aminotransferase), and (F) Cre (creatinine) were measured. Results are expressed as mean ± SEM (n=5). $^{\#}p<0.05$ vs. PBS group. ns, not significant.

References

1. Chen, J., Huang, Q., Li, J., Yao, Y., Sun, W., Zhang, Z., Qi, H., Chen, Z., Liu, J., Zhao, D., Mi, J., & Li, X. (2023). Panax ginseng against myocardial ischemia/reperfusion injury: A review of preclinical evidence and potential mechanisms. *Journal of Ethnopharmacology*, *300*. https://doi.org/10.1016/j.jep.2022.115715
2. Huang, L., Li, H. J., & Wu, Y. C. (2023). Processing technologies, phytochemistry, bioactivities and applications of black ginseng-a novel manufactured ginseng product: A comprehensive review. *Food Chemistry*, *407*, 134714. https://doi.org/10.1016/j.foodchem.2022.134714
3. Fan, S., Zhang, Z., Su, H., Xu, P., Qi, H., Zhao, D., & Li, X. (2020). Panax ginseng clinical trials: Current status and future perspectives. *Biomedicine and Pharmacotherapy*, *132*, 110832. https://doi.org/10.1016/j.biopha.2020.110832
4. He, Y., Yang, J., Lv, Y., Chen, J., Yin, F., Huang, J., & Zheng, Q. (2018). A Review of Ginseng Clinical Trials Registered in the WHO International Clinical Trials Registry Platform. *Biomed Res Int*, *2018*, 1843142. https://doi.org/10.1155/2018/1843142
5. Tan, J., Zhang, H., Zhang, L., & Xu, H. (2023). Ginseng and "Shanghuo" (fireness): a comprehensive review from the viewpoints of TCM theory and modern science. *Food & Function*, *14*(8), 3437-3453. https://doi.org/10.1039/d2fo03873k

6. Chen, W., Yao, P., Vong, C. T., Li, X., Chen, Z., Xiao, J., Wang, S., & Wang, Y. (2021). Ginseng: A bibliometric analysis of 40-year journey of global clinical trials. *J Adv Res*, *34*, 187-197. https://doi.org/10.1016/j.jare.2020.07.016

7. Tao, R., Lu, K., Zong, G., Xia, Y., Han, H., Zhao, Y., Wei, Z., & Lu, Y. (2023). Ginseng polysaccharides: Potential antitumor agents. *J Ginseng Res*, *47*(1), 9-22. https://doi.org/10.1016/j.jgr.2022.07.002

8. Liu, H., Xie, T., & Liu, Y. (2023). Ginsenoside Rg3 inhibits the malignant progression of cervical cancer cell by regulating AKT2 expression. *Heliyon*, *9*(8), e19045. https://doi.org/10.1016/j.heliyon.2023.e19045

9. Yang, C., Qian, C., Zheng, W., Dong, G., Zhang, S., Wang, F., Wei, Z., Xu, Y., Wang, A., Zhao, Y., & Lu, Y. (2024). Ginsenoside Rh2 enhances immune surveillance of natural killer (NK) cells via inhibition of ERp5 in breast cancer. *Phytomedicine*, *123*, 155180. https://doi.org/10.1016/j.phymed.2023.155180

10. Zhou, X., Shi, H., Jiang, G., Zhou, Y., & Xu, J. (2014). Antitumor activities of ginseng polysaccharide in C57BL/6 mice with Lewis lung carcinoma. *Tumour Biology*, *35*(12), 12561-12566. https://doi.org/10.1007/s13277-014-2576-7

11. Li, A., Li, D., Gu, Y., Liu, R., Tang, X., Zhao, Y., Qi, F., Wei, J., & Liu, J. (2023). Plant-derived nanovesicles: Further exploration of biomedical function and

application potential. *Acta Pharm Sin B*, *13*(8), 3300-3320. https://doi.org/10.1016/j.apsb.2022.12.022

12. Suharta, S., Barlian, A., Hidajah, A. C., Notobroto, H. B., Ana, I. D., Indariani, S., Wungu, T. D. K., & Wijaya, C. H. (2021). Plant-derived exosome-like nanoparticles: A concise review on its extraction methods, content, bioactivities, and potential as functional food ingredient. *Journal of Food Science*, *86*(7), 2838-2850. https://doi.org/10.1111/1750-3841.15787
13. Feng, J., Xiu, Q., Huang, Y., Troyer, Z., Li, B., & Zheng, L. (2023). Plant-Derived Vesicle-Like Nanoparticles as Promising Biotherapeutic Tools: Present and Future. *Adv Mater*, *35*(24), e2207826. https://doi.org/10.1002/adma.202207826
14. Lian, M. Q., Chng, W. H., Liang, J., Yeo, H. Q., Lee, C. K., Belaid, M., Tollemeto, M., Wacker, M. G., Czarny, B., & Pastorin, G. (2022). Plant-derived extracellular vesicles: Recent advancements and current challenges on their use for biomedical applications. *J Extracell Vesicles*, *11*(12), e12283. https://doi.org/10.1002/jev2.12283
15. Xu, Z., Xu, Y., Zhang, K., Liu, Y., Liang, Q., Thakur, A., Liu, W., & Yan, Y. (2023). Plant-derived extracellular vesicles (PDEVs) in nanomedicine for human disease and therapeutic modalities. *J Nanobiotechnology*, *21*(1), 114. https://doi.org/10.1186/s12951-023-01858-7

16. Cao, M., Yan, H., Han, X., Weng, L., Wei, Q., Sun, X., Lu, W., Wei, Q., Ye, J., Cai, X., Hu, C., Yin, X., & Cao, P. (2019). Ginseng-derived nanoparticles alter macrophage polarization to inhibit melanoma growth. *J Immunother Cancer*, *7*(1), 326. https://doi.org/10.1186/s40425-019-0817-4

17. Han, X., Wei, Q., Lv, Y., Weng, L., Huang, H., Wei, Q., Li, M., Mao, Y., Hua, D., Cai, X., Cao, M., & Cao, P. (2022). Ginseng-derived nanoparticles potentiate immune checkpoint antibody efficacy by reprogramming the cold tumor microenvironment. *Molecular Therapy*, *30*(1), 327-340. https://doi.org/10.1016/j.ymthe.2021.08.028

18. Kim, J., Zhang, S., Zhu, Y., Wang, R., & Wang, J. (2023). Amelioration of colitis progression by ginseng-derived exosome-like nanoparticles through suppression of inflammatory cytokines. *Journal of Ginseng Research*, *47*(5), 627-637. https://doi.org/10.1016/j.jgr.2023.01.004

19. Lv, Y., Li, M., Weng, L., Huang, H., Mao, Y., Yang, D. A., Wei, Q., Zhao, M., Wei, Q., Rui, K., Han, X., Fan, W., Cai, X., Cao, P., & Cao, M. (2023). Ginseng-derived nanoparticles reprogram macrophages to regulate arginase-1 release for ameliorating T cell exhaustion in tumor microenvironment. *Journal of Experimental and Clinical Cancer Research*, *42*(1), 322. https://doi.org/10.1186/s13046-023-02888-7

20. Wang, H., Mu, J., Chen, Y., Liu, Y., Li, X., Li, H., & Cao, P. (2024). Hybrid Ginseng-

726 derived Extracellular Vesicles-Like Particles with Autologous Tumor Cell Membrane
727 for Personalized Vaccination to Inhibit Tumor Recurrence and Metastasis. *Adv Sci*
728 *(Weinh)*, *11*(17), e2308235. https://doi.org/10.1002/advs.202308235
729 21. Yang, L., Jin, W. Q., Tang, X. L., Zhang, S., Ma, R., Zhao, D. Q., & Sun, L. W. (2022).
730 Ginseng-derived nanoparticles inhibit lung cancer cell epithelial mesenchymal
731 transition by repressing pentose phosphate pathway activity. *Frontiers in Oncology*,
732 *12*, 942020. https://doi.org/10.3389/fonc.2022.942020
733 22. Cho, E. G., Choi, S. Y., Kim, H., Choi, E. J., Lee, E. J., Park, P. J., Ko, J., Kim, K. P.,
734 & Baek, H. S. (2021). Panax ginseng-Derived Extracellular Vesicles Facilitate Anti-
735 Senescence Effects in Human Skin Cells: An Eco-Friendly and Sustainable Way to
736 Use Ginseng Substances. *Cells*, *10*(3). https://doi.org/10.3390/cells10030486
737 23. Choi, W., Cho, J. H., Park, S. H., Kim, D. S., Lee, H. P., Kim, D., Kim, H. S., Kim, J.
738 H., & Cho, J. Y. (2024). Ginseng root-derived exosome-like nanoparticles protect skin
739 from UV irradiation and oxidative stress by suppressing activator protein-1 signaling
740 and limiting the generation of reactive oxygen species. *J Ginseng Res*, *48*(2), 211-219.
741 https://doi.org/10.1016/j.jgr.2024.01.001
742 24. Park, H. Y., Kang, M. H., Lee, G., & Kim, J. W. (2025). Enhancement of skin
743 regeneration through activation of TGF-β/SMAD signaling pathway by Panax

744 ginseng meyer non-edible callus-derived extracellular vesicles. *Journal of Ginseng*
745 *Research*, *49*(1), 34-41. https://doi.org/10.1016/j.jgr.2024.08.002.
746 25. Kim, J., Zhu, Y., Chen, S., Wang, D., Zhang, S., Xia, J., Li, S., Qiu, Q., Lee, H., &
747 Wang, J. (2023). Anti-glioma effect of ginseng-derived exosomes-like nanoparticles
748 by active blood-brain-barrier penetration and tumor microenvironment modulation. *J*
749 *Nanobiotechnology*, *21*(1), 253. https://doi.org/10.1186/s12951-023-02006-x
750 26. Li, T., Wang, H., Bi, W., Su, Y., Xiong, Y., Wang, S., & Han, L. (2024). Nano-
751 Characterization, Composition Analysis, and Anti-Inflammatory Activity of
752 American-Ginseng-Derived Vesicle-like Nanoparticles. *Molecules*, *29*(15).
753 https://doi.org/10.3390/molecules29153443
754 27. Ma, C., Liu, K., Wang, F., Fei, X., Niu, C., Li, T., & Liu, L. (2024). Neutrophil
755 membrane-engineered Panax ginseng root-derived exosomes loaded miRNA 182-5p
756 targets NOX4/Drp-1/NLRP3 signal pathway to alleviate acute lung injury in sepsis:
757 experimental studies. *International Journal of Surgery (London, England)*, *110*(1),
758 72-86. https://doi.org/10.1097/JS9.0000000000000789
759 28. Yang, S., Li, W., Bai, X., Di Nunzio, G., Fan, L., Zhao, Y., Ren, L., Zhao, R., Bian,
760 S., Liu, M., Wei, Y., Zhao, D., & Wang, J. (2024). Ginseng-derived nanoparticles
761 alleviate inflammatory bowel disease via the TLR4/MAPK and p62/Nrf2/Keap1

762 pathways. *J Nanobiotechnology*, *22*(1), 48. https://doi.org/10.1186/s12951-024-
763 02313-x
764 29. Hyoudou, K., Nishikawa, M., Umeyama, Y., Kobayashi, Y., Yamashita, F., &
765 Hashida1, M. (2004). Inhibition of Metastatic Tumor Growth in Mouse Lung by
766 Repeated Administration of Polyethylene Glycol-Conjugated Catalase: Quantitative
767 Analysis with Firefly Luciferase-Expressing Melanoma Cells. *Clinical Cancer*
768 *Research*, *10*, 7685-7691. https://doi.org/10.1158/1078-0432.CCR-04-1020
769 30. Nishinaka T., Mori S., Yamazaki Y., Niwa A., Wake H., Yoshino T., Nishibori M.,
770 Takahashi H. (2020). A comparative study of sulphated polysaccharide effects on
771 advanced glycation end-product uptake and scavenger receptor class A level in
772 macrophages. *Diab Vasc Dis Res*. 17(1), 1479164119896975.
773 https://doi.org/10.1177/1479164119896975
774 31. Takeda H., Nakajima Y., Yamaguchi T., Watanabe I., Miyoshi S., Nagashio K., Sekine
775 H., Motohashi H., Yano H., Tanaka J. (2023). The anti-inflammatory and anti-
776 oxidative effect of a classical hypnotic bromovalerylurea mediated by the activation
777 of NRF2. *J Biochem.* 174(2), 131-142. https://doi.org/10.1093/jb/mvad030.
778 32. Noguchi, T., Michihata, T., Nakamura, W., Takumi, T., Shimizu, R., Yamamoto, M.,
779 Ikeda, M., Ohmiya, Y., and Nakajima, Y. (2010) Dual-color luciferase mouse directly

780 demonstrates coupled expression of two clock genes. Biochemistry 49, 8053–8061.
781 doi: https://doi.org/10.1021/bi100545h
782 33. Kanda, Y. (2013). Investigation of the freely available easy-to-use software 'EZR' for
783 medical statistics. *Bone Marrow Transplantation*, *48*(3), 452-458.
784 https://doi.org/10.1038/bmt.2012.244
785 34. Jie, Y., He, W., Yang, X., & Chen, W. (2017). Kruppel-like factor 4 acts as a potential
786 therapeutic target of Sijunzi decoction for treatment of colorectal cancer. *Cancer Gene*
787 *Therapy*, *24*(9), 361-366. https://doi.org/10.1038/cgt.2017.25
788 35. Ju, S., Mu, J., Dokland, T., Zhuang, X., Wang, Q., Jiang, H., Xiang, X., Deng, Z. B.,
789 Wang, B., Zhang, L., Roth, M., Welti, R., Mobley, J., Jun, Y., Miller, D., & Zhang, H.
790 G. (2013). Grape exosome-like nanoparticles induce intestinal stem cells and protect
791 mice from DSS-induced colitis. *Molecular Therapy*, *21*(7), 1345-1357.
792 https://doi.org/10.1038/mt.2013.64
793 36. Mu, J., Zhuang, X., Wang, Q., Jiang, H., Deng, Z. B., Wang, B., Zhang, L., Kakar, S.,
794 Jun, Y., Miller, D., & Zhang, H. G. (2014). Interspecies communication between plant
795 and mouse gut host cells through edible plant derived exosome-like nanoparticles.
796 *Molecular Nutrition & Food Research*, *58*(7), 1561-1573.
797 https://doi.org/10.1002/mnfr.201300729

37. Iitsuka, H., Koizumi, K., Inujima, A., Suzaki, M., Mizuno, Y., Takeshita, Y., Eto, T., Otsuka, Y., Shimada, R., Liu, M., Ikeda, K., Nakano, M., Suzuki, R., Maruyama, K., Zhou, Y., Sakurai, H., & Shibahara, N. (2018). Discovery of a sugar-based nanoparticle universally existing in boiling herbal water extracts and their immunostimulant effect. *Biochem Biophys Rep*, *16*, 62-68. https://doi.org/10.1016/j.bbrep.2018.08.004

38. Kawada, K., Ishida, T., Morisawa, S., Jobu, K., Higashi, Y., Aizawa, F., Yagi, K., Izawa-Ishizawa, Y., Niimura, T., Abe, S., Goda, M., Miyamura, M., & Ishizawa, K. (2024). Atractylodes lancea (Thunb.) DC. [Asteraceae] rhizome-derived exosome-like nanoparticles suppress lipopolysaccharide-induced inflammation in murine microglial cells. *Frontiers in Pharmacology*, *15*, 1302055. https://doi.org/10.3389/fphar.2024.1302055

39. Karamanidou, T., & Tsouknidas, A. (2021). Plant-Derived Extracellular Vesicles as Therapeutic Nanocarriers. *International Journal of Molecular Sciences*, *23*(1). https://doi.org/10.3390/ijms23010191

40. Kim, J., Li, S., Zhang, S., & Wang, J. (2022). Plant-derived exosome-like nanoparticles and their therapeutic activities. *Asian J Pharm Sci*, *17*(1), 53-69. https://doi.org/10.1016/j.ajps.2021.05.006

816 41. Caffall, K. H., & Mohnen, D. (2009). The structure, function, and biosynthesis of
817 plant cell wall pectic polysaccharides. *Carbohydrate Research*, *344*(14), 1879-1900.
818 https://doi.org/10.1016/j.carres.2009.05.021
819 42. Moore, J. P., Farrant, J. M., & Driouich, A. (2008). A role for pectin-associated
820 arabinans in maintaining the flexibility of the plant cell wall during water deficit stress.
821 *Plant Signaling & Behavior*, *3*(2), 102-104.
822 43. Wang, D., Lv, Y., Xu, L., Bu, H., & Li, X. (2011). Content determination of
823 polysaccharide in the root of Panax ginseng. *China Journal of Traditional Chinese*
824 *Medicine and Pharmacy*, *26*, 774-776.
825 44. Sun, L., Ropartz, D., Cui, L., Shi, H., Ralet, M. C., & Zhou, Y. (2019). Structural
826 characterization of rhamnogalacturonan domains from Panax ginseng C. A. Meyer.
827 *Carbohydr Polym*, *203*, 119-127. https://doi.org/10.1016/j.carbpol.2018.09.045
828 45. Akira, S., Uematsu, S., & Takeuchi, O. (2006). Pathogen recognition and innate
829 immunity. *Cell*, *124*(4), 783-801. https://doi.org/10.1016/j.cell.2006.02.015
830 46. Laird, M. H., Rhee, S. H., Perkins, D. J., Medvedev, A. E., Piao, W., Fenton, M. J., &
831 Vogel, S. N. (2009). TLR4/MyD88/PI3K interactions regulate TLR4 signaling.
832 *Journal of Leukocyte Biology*, *85*(6), 966-977. https://doi.org/10.1189/jlb.1208763
833 47. Chen, I. T., Cheng A. C., Liu Y. T., Yan C., Cheng Y. C., Chang C. F., Tseng P. H.

(2022). Persistent TLR4 Activation Promotes Hepatocellular Carcinoma Growth through Positive Feedback Regulation by LIN28A/Let-7g miRNA. *Int J Mol Sci.* 23(15), 8419. https://doi.org/10.3390/ijms23158419.

48. Barnes, P. J. (1997). Nuclear Factor-lcB. *ht. J. Biochem. cell Bid.*, *29*(6), 867-887.

49. Lee, J. I., & Burckart, G. J. (1998). Nuclear factor kappa B: important transcription factor and therapeutic target. *Journal of Clinical Pharmacology*, *38*(11), 981-993. https://doi.org/10.1177/009127009803801101

50. Liu, T., Zhang, L., Joo, D., & Sun, S. C. (2017). NF-kappaB signaling in inflammation. *Signal Transduct Target Ther*, *2*, 17023-. https://doi.org/10.1038/sigtrans.2017.23

51. Guttridge, D. C., Albanese, C., Reuther, J. Y., Pestell, R. G., & Jr, A. S. B. (1999). NF-kB Controls Cell Growth and Differentiation through Transcriptional Regulation of Cyclin D1. *Molecular and Cellular Biology*, *19*(8), 5785–5799.

52. Zhu, F., Yue, W., & Wang, Y. (2014). The nuclear factor kappa B (NF-kappaB) activation is required for phagocytosis of staphylococcus aureus by RAW 264.7 cells. *Experimental Cell Research*, *327*(2), 256-263. https://doi.org/10.1016/j.yexcr.2014.04.018

53. Edberg, J. C., Lin, C. T., Lau, D., Unkeless, J. C., & Kimberly, R. P. (1995). The Ca^{2+} dependence of human Fc gamma receptor-initiated phagocytosis. *The Journal of*

852 *biological chemistry*, 270(38), 22301–22307.
853 https://doi.org/10.1074/jbc.270.38.22301
854 54. Yang, S., Min, C., Moon, H., Moon, B., Lee, J., Jeon, J., Kwon, H., Jang, D., & Park,
855 D. (2023). Internalization of apoptotic cells during efferocytosis requires Mertk-
856 mediated calcium influx. *Cell death & disease*, 14(6), 391.
857 https://doi.org/10.1038/s41419-023-05925-7
858 55. Yu H., Ha T., Liu L., Wang X., Gao M., Kelley J., Kao R., Williams D., Li C. (2012).
859 Scavenger receptor A (SR-A) is required for LPS-induced TLR4 mediated NF-κB
860 activation in macrophages. *Biochim Biophys Acta.* 1823(7), 1192-8.
861 https://doi.org/10.1016/j.bbamcr.2012.05.004.
862 56. Platt N., & Gordon S. Is the class A macrophage scavenger receptor (SR-A)
863 multifunctional? - The mouse's tale. (2001). *J Clin Invest*. 108(5), 649-54.
864 https://doi.org/10.1172/JCI13903.
865 57. Doi, T., Higashino, K., Kurihara, Y., Wada, Y., Miyazaki, T., Nakamura, H., Uesugi,
866 S., Imanishi, T., Kawabe, Y., Itakur,a H., Yazaki, Y., matsumoto, A., & Kodama, T.
867 (1993). Charged collagen structure mediates the recognition of negatively charged
868 macromolecules by macrophage scavenger receptors. *J Biol Chem*. 268(3), 2126-33.
869 https://doi.org/10.1016/S0021-9258(18)53971-5

58. Haabeth, O. A., Bogen, B., & Corthay, A. (2012). A model for cancer-suppressive inflammation. *Oncoimmunology*, *1*(7), 1146-1155. https://doi.org/10.4161/onci.21542

59. Kloosterman, D. J., & Akkari, L. (2023). Macrophages at the interface of the co-evolving cancer ecosystem. *Cell*, *186*(8), 1627-1651. https://doi.org/10.1016/j.cell.2023.02.020

60. Li, Z., Wang, Y. J., Zhou, J., Umakoshi, M., & Goto, A. (2022). The prognostic role of M2 tumor-associated macrophages in non-small-cell lung cancer. *Histology and Histopathology*, *37*(12), 1167-1175. https://doi.org/10.14670/HH-18-474

61. Hobbs, S., Reynoso, M., Geddis, A. V., Mitrophanov, A. Y., & Matheny, R. W., Jr. (2018). LPS-stimulated NF-kappaB p65 dynamic response marks the initiation of TNF expression and transition to IL-10 expression in RAW 264.7 macrophages. *Physiol Rep*, *6*(21), e13914. https://doi.org/10.14814/phy2.13914

62. Zhang, H., & Kuchroo, V. (2019). Epigenetic and transcriptional mechanisms for the regulation of IL-10. *Seminars in Immunology*, *44*, 101324. https://doi.org/10.1016/j.smim.2019.101324

63. Kienzl, M., Maitz, K., Sarsembayeva, A., Valadez-Cosmes, P., Gruden, E., Ristic, D., Herceg, K., Kargl, J., & Schicho, R. (2024). Comparative Study of the Immune

888 Microenvironment in Heterotopic Tumor Models. *Cancers*, *16*(2).
889 https://doi.org/10.3390/cancers16020295
890 64. Lelliott, E. J., Cullinane, C., Martin, C. A., Walker, R., Ramsbottom, K. M., Souza-
891 Fonseca-Guimaraes, F., Abuhammad, S., Michie, J., Kirby, L., Young, R. J., Slater,
892 A., Lau, P., Meeth, K., Oliaro, J., Haynes, N., McArthur, G. A., & Sheppard, K. E.
893 (2019). A novel immunogenic mouse model of melanoma for the preclinical
894 assessment of combination targeted and immune-based therapy. *Scientific Reports*,
895 *9*(1), 1225. https://doi.org/10.1038/s41598-018-37883-y
896 65. Trocchia, M., Ventrici, A., Modestino, L., Cristinziano, L., Ferrara, A. L., Palestra, F.,
897 Loffredo, S., Capone, M., Madonna, G., Romanelli, M., Ascierto, P. A., & Galdiero,
898 M. R. (2024). Innate Immune Cells in Melanoma: Implications for Immunotherapy.
899 *International Journal of Molecular Sciences*, *25*(15).
900 https://doi.org/10.3390/ijms25158523
901 66. Ji, S., Lee, J., Lee, E. S., Kim, D. H., & Sin, J. I. (2021). B16 melanoma control by
902 anti-PD-L1 requires CD8+ T cells and NK cells: application of anti-PD-L1 Abs and
903 Trp2 peptide vaccines. *Human Vaccines & Immunotherapeutics*, *17*(7), 1910-1922.
904 https://doi.org/10.1080/21645515.2020.1866951
905 67. Laskin, D. L., Weinberger, B., & Laskin, J. D. (2001). Functional heterogeneity in

liver and lung macrophages. *Journal of Leukocyte Biology*, *70*(2), 163-170. https://doi.org/10.1189/jlb.70.2.163

68. Lin, Z., Zhang, Y., Cai, H., Zhou, F., Gao, H., Deng, L., & Li, R. (2019). A PD-L1-Based Cancer Vaccine Elicits Antitumor Immunity in a Mouse Melanoma Model. *Mol Ther Oncolytics*, *14*, 222-232. https://doi.org/10.1016/j.omto.2019.06.002

69. Cao, Z., Joseph, W. R., Browne, W. L., Mountjoy, K. G., Palmer, B. D., Baguley, B. C., & Ching, L. M. (1999). Thalidomide increases both intra-tumoural tumour necrosis factor-alpha production and anti-tumour activity in response to 5,6-dimethylxanthenone-4-acetic acid. *British Journal of Cancer*, *80*(5-6), 716-723. https://doi.org/10.1038/sj.bjc.6690415

70. Manda, T., Shimomura, K., Mukumoto, S., Kobayashi, K., Mizota, T., Hirai, O., Matsumoto, S., Oku, T., Nishigaki, F., Mori, J., & et al. (1987). Recombinant human tumor necrosis factor-alpha: evidence of an indirect mode of antitumor activity. *Cancer Research*, *47*(14), 3707-3711. https://www.ncbi.nlm.nih.gov/pubmed/3594435

71. den Haan, J. M., & Kraal, G. (2012). Innate immune functions of macrophage subpopulations in the spleen. *Journal of Innate Immunity*, *4*(5-6), 437-445. https://doi.org/10.1159/000335216

924 72. Lewis, S. M., Williams, A., & Eisenbarth, S. C. (2019). Structure and function of the
925 immune system in the spleen. *Sci Immunol*, *4*(33).
926 https://doi.org/10.1126/sciimmunol.aau6085
927 73. Steiner, K., Waase, I., Rau, T., Dietrich, M., Fleischer, B., & Broker, B. M. (1999).
928 Enhanced expression of CTLA-4 (CD152) on CD4+ T cells in HIV infection. *Clinical*
929 *and Experimental Immunology*, *115*(3), 451-457. https://doi.org/10.1046/j.1365-
930 2249.1999.00806.x
931 74. Saibil, S. D., & Ohashi, P. S. (2020). Targeting T cell activation in immuno-oncology.
932 *Current Oncology (Toronto, Ont.)*, *27*(Suppl 2), S98-S105.
933 https://doi.org/10.3747/co.27.5285
934 75. Yoshimura, S., Bondeson, J., Brennan, F. M., Foxwell, B. M., & Feldmann, M. (2001).
935 Role of NFkappaB in antigen presentation and development of regulatory T cells
936 elucidated by treatment of dendritic cells with the proteasome inhibitor PSI. *European*
937 *Journal of Immunology*, *31*(6), 1883-1893. https://doi.org/10.1002/1521-
938 4141(200106)31:6<1883::aid-immu1883>3.0.co;2-v
939 76. Yoshimura, S., Bondeson, J., Foxwell, B. M., Brennan, F. M., & Feldmann, M. (2001).
940 Effective antigen presentation by dendritic cells is NF-kappaB dependent: coordinate
941 regulation of MHC, co-stimulatory molecules and cytokines. *International*

Immunology, *13*(5), 675-683. https://doi.org/10.1093/intimm/13.5.675

77. Bae, J., Koo, J., Kim, S., Park, T. Y., & Kim, M. Y. (2012). Ginsenoside Rp1 Exerts Anti-inflammatory Effects via Activation of Dendritic Cells and Regulatory T Cells. *J Ginseng Res*, *36*(4), 375-382. https://doi.org/10.5142/jgr.2012.36.4.375

78. Takei, M., Tachikawa, E., Hasegawa, H., & Lee, J. J. (2004). Dendritic cells maturation promoted by M1 and M4, end products of steroidal ginseng saponins metabolized in digestive tracts, drive a potent Th1 polarization. *Biochemical Pharmacology*, *68*(3), 441-452. https://doi.org/10.1016/j.bcp.2004.04.015

Supplementary Files

This is a list of supplementary files associated with this preprint. Click to download.

- SupplementaryFin261109.docx